Analyses of [^{18}F]Altanserin Bolus Injection PET Data. I: Consideration of Radiolabeled Metabolites in Baboons

JULIE C. PRICE,* BRIAN J. LOPRESTI, NEALE S. MASON, DANIEL P. HOLT, Y. HUANG, AND CHESTER A. MATHIS

Department of Radiology, University of Pittsburgh School of Medicine, Pittsburgh, Pennsylvania

KEY WORDS positron emission tomography (PET); [^{18}F]altanserin; serotonin receptor; 5-HT$_{2A}$; imaging

ABSTRACT Positron emission tomography (PET) has been used to study serotonin 2A (5-HT$_{2A}$) receptor binding in human brain using the 5-HT$_{2A}$ antagonist, [^{18}F]altanserin. Previous analyses of bolus injection [^{18}F]altanserin data provided 5-HT$_{2A}$ specific binding measures that were highly correlated with the in vitro distribution of 5-HT$_{2A}$ receptors and reflected decreased binding after ketanserin (5-HT$_{2A}$ antagonist) administration. These observations were made in the presence of a nonspecific tissue component that was consistent with blood–brain barrier (BBB) passage of radiolabeled metabolites (radiometabolites). In this work, we evaluated the in vivo kinetics of [^{18}F]altanserin and two major radiometabolites of [^{18}F]altanserin, focusing on the kinetics of free and nonspecifically-bound radioactivity. PET studies were performed in baboons after the bolus injection of [^{18}F]altanserin or one of its major radiometabolites, either [^{18}F]altanserinol or [^{18}F]4-(4-fluorobenzoyl)piperidine, at baseline and after pharmacologic receptor blockade (blocking data). The cerebellar and blocking data were analyzed using either single (parent radiotracer) or dual (parent radiotracer and radiometabolites) input function methods. After bolus injection of either [^{18}F]altanserin metabolite, radioactivity crossed the BBB and localized nonspecifically. The radiometabolites were found to contribute to nonspecific "background" radioactivity that was similar in receptor-poor and receptor-rich regions. After bolus injection in baboons, two of the major radiometabolites of [^{18}F]altanserin crossed the BBB and contributed to a fairly uniform background of nonspecific radioactivity. This uniformity suggests that conventional analyses are appropriate for human bolus injection [^{18}F]altanserin PET data, although these methods may overestimate [^{18}F]altanserin nonspecific binding. **Synapse 41:1–10, 2001.**

INTRODUCTION

Positron emission tomography (PET) studies of the serotonin 2A receptor subtype (5-HT$_{2A}$) have been performed in humans using the 5-HT$_{2A}$ antagonist [^{18}F]altanserin (Lemaire et al., 1991). These PET studies were quantified by conventional kinetic methods that relied on one input function (unmetabolized [^{18}F]altanserin only) to describe the regional kinetics of [^{18}F]altanserin in brain (Biver et al., 1994; Sadzot et al., 1995). Application of these analyses yielded regional 5-HT$_{2A}$ receptor binding measures that followed the in vitro rank order of 5-HT$_{2A}$ receptor density and reflected displacement of [^{18}F]altanserin by ketanserin (5-HT$_{2A}$ antagonist), while a test-retest variability of about 10% was achievable (Biver et al., 1994; Sadzot et al., 1995; Smith et al., 1998).

The compartmental analyses of [^{18}F]altanserin PET data, acquired after bolus injection, indicated the existence of a slow nonspecific binding component that was most evident in the cerebellar data (5-HT$_{2A}$ receptor-poor region) for which the PET value at 90 min was approximately 40% of the peak PET value (Biver et al., 1994; Sadzot et al., 1995). Preliminary applications of a metabolite model that relied on two input functions ([^{18}F]altanserin and radiolabeled metabolites) and allowed for blood–brain barrier (BBB) passage of radiolabeled metabolites (radiometabolites) indicated that

Contract grant sponsor: NIH; Contract grant numbers: MH52247, NS22899, MH42984, MH49936, MH01410.

*Correspondence to: Dr. Julie C. Price, PET Facility, Department of Radiology, 200 Lothrop St., Rm. B938, Pittsburgh, PA 15213. E-mail: price@pet.upmc.edu

Received 16 August 2000; Accepted 20 December 2000

this nonspecific component was consistent with uptake of radiolabeled metabolites (Mintun et al., 1996; Price et al., 1998). In addition, this model provided a good description of the regional [^{18}F]altanserin tissue kinetics.

Efforts were undertaken in animals and humans to characterize the radiolabeled metabolites of [^{18}F]altanserin (Smith et al., 1998; Lopresti et al., 1998; Price et al., 1998; Tan et al., 1999). These studies were aimed at obtaining a better understanding of the in vivo kinetics of the metabolites of [^{18}F]altanserin and to examine the validity of the conventional "single-input" methods. For example, a step-gradient HPLC analysis of rat plasma after the injection of [^{18}F]altanserin yielded four major radiolabeled metabolites of [^{18}F]altanserin (Smith et al., 1998). These studies included ex vivo tissue assays in rats which showed that three of these radiolabeled metabolites crossed the BBB and localized nonspecifically throughout the brain, although only two (later identified as [^{18}F]altanserinol and a metabolite of [^{18}F]4-(4-fluorobenzoyl)piperidine) significantly contributed to the total measured brain radioactivity.

The primary aim of the present work was to investigate the [^{18}F]altanserin nonspecific binding component in nonhuman primates by performing PET studies of two significant radiolabeled metabolites of [^{18}F]altanserin. These studies were performed to obtain a better understanding of how these radiolabeled metabolites might impact the validity of the conventional analyses of bolus injection data. Quantitative PET studies were performed in baboons after the bolus injection of [^{18}F]altanserin or one of the radiolabeled metabolites of [^{18}F]altanserin, either [^{18}F]altanserinol or [^{18}F]4-(4-fluorobenzoyl)piperidine.

MATERIALS AND METHODS

Radiochemistry

[^{18}F]Altanserin

The radiosynthesis of [^{18}F]altanserin was performed using the previously described method of Lemaire et al. (1991) to provide end of synthesis (EOS) yields of 15–20% (30–40 mCi), EOS specific activities of about 2,000 Ci/mmol, and final product chemical and radiochemical purities of greater than 95% following an 80-min synthesis.

[^{18}F]Altanserinol ([^{18}F]ALT-ol)

[^{18}F]ALT-ol (a secondary alcohol), a metabolite of [^{18}F]altanserin, is likely formed in vivo by reduction of the ketone functionality in [^{18}F]altanserin in a manner analogous to that reported for ketanserin, a close structural analog of altanserin (Heykants et al., 1988). [^{18}F]ALT-ol was synthesized from [^{18}F]altanserin using a reaction mixture consisting of [^{18}F]altanserin in 1 mL of absolute ethanol added to a V-vial containing 10 mg of sodium borohydride. The mixture was allowed to react for 1 min at room temperature and the reaction was terminated by the addition of water. [^{18}F]ALT-ol was purified by reverse-phase high performance liquid chromatography (HPLC) (Waters μBondapak C_{18} column; 7.8 × 300 mm; 22% acetonitrile/78% 0.29 M acetic acid/0.03 M ammonium acetate; pH 5.2). The radioactivity corresponding to [^{18}F]ALT-ol was collected, diluted with water, and transferred to an activated C_{18} Sep-Pak cartridge. The Sep-Pak was washed with water and the residual activity was eluted with 1 mL of ethanol, filtered, and diluted with saline for injection. The final product was obtained following a 2-h synthesis with EOS yields of 6 ± 2% (based on starting [^{18}F]fluoride). The material obtained was greater than 95% chemically and radiochemically pure with a specific activity in excess of 2,000 Ci/mmol at EOS.

[^{18}F]4-(4-fluorobenzoyl)piperidine ([^{18}F]4-FBP)

[^{18}F]4-FBP, a metabolite of [^{18}F]altanserin, is likely formed in vivo by the N-dealkylation of [^{18}F]altanserin, analogous to the metabolic route of ketanserin (Heykants et al., 1988). [^{18}F]4-FBP was synthesized using an ^{18}F-for-NO_2 displacement reaction with 4-(4-nitrobenzoyl)piperidine as the starting material (Mason et al., 1997). Five mg of 4-(4-nitrobenzoyl)piperidine were dissolved in 1 mL of anhydrous DMSO and added to Kryptofix[222]/K_2CO_3 and [^{18}F]fluoride previously dried by repeated azeotropic distillations with acetonitrile in a V-vial. The vial was sealed and subjected to microwave irradiation for 2.3 min at 600 watts. The crude reaction mixture was diluted with 1 mL of water and purified by HPLC (Waters μBondapak C_{18} column; 7.8 × 300 mm; 15% acetonitrile/85% 0.29 M acetic acid/0.03 M ammonium acetate; pH 5.2). The radioactivity corresponding to [^{18}F]4-FBP was collected, diluted with water, and transferred to an activated C_{18} Sep-Pak cartridge. The Sep-Pak was washed with water and the residual activity was eluted with 1 mL of ethanol, filtered, and diluted with saline for injection. The final product was obtained in approximately 75 min with an EOS yield of ~35%. The material obtained was greater than 90% chemically and 95% radiochemically pure with an EOS specific activity in excess of 2,000 Ci/mmol.

All radiotracer studies were carried out at high specific activity (>1,500 Ci/mmol) and it was assumed that the occupation of receptor sites by unlabeled tracer was negligible. Verification of the chemical identity of the compounds was based on their identical chromatographic properties compared to those of authentic, unlabeled (cold) altanserin, ALT-ol, or 4-FBP. Altanserin was provided by Janssen Pharmaceuticals (Beerse, Belgium) and ALT-ol and 4-FBP were synthesized in-house. The chemical identities of ALT-ol and 4-FBP were confirmed using high-field (300 MHz) proton nuclear magnetic resonance spectroscopy and gas chromatography-mass spectrometry analyses.

Imaging

PET data were acquired in 2D imaging mode using an ECAT 951R/31 PET scanner (CTI PET Systems, Knoxville, TN). This instrument simultaneously acquired 31 image planes (axial field of view: 10.5 cm) with a transaxial resolution of 5.8 mm FWHM (ramp filter). Each of the PET radiotracers was administered i.v. over 20 sec. A dynamic series of PET scans were acquired over either 90 or 120 min with 20–23 frames. Emission data were corrected for attenuation, dead time, and radioactive decay. A thorough description and discussion of the application of this PET scanner to studies in baboons has been published previously (Drevets et al., 1999).

The animal studies were conducted with the approval of the local Institutional Animal Care and Use Committee. Prior to PET imaging, baboons (*Papio anubis*) were administered ketamine (15 mg/kg) and atropine (0.5 mg) i.m. to anesthetize the animals and to control heart rate. Pancuronium bromide was administered as necessary to keep the animals immobilized during the study. Baboons were maintained on isoflurane (0.5–1.25%) anesthesia and ventilated with medical air while expired CO_2, blood pressure, and heart rate were monitored. The body temperature of the baboons was regulated and monitored using a Gaymar® blanket (Orchard Park, NY) and Yellow Springs Instruments temperature regulator (YSI®, Yellow Springs, Ohio). PET studies were performed following high specific activity bolus injections of [^{18}F]altanserin (10–30 mCi), [^{18}F]ALT-ol (~10 mCi), or [^{18}F]4-FBP (~10 mCi) with the following sequence of frames: 6 × 30 sec, 1 × 1 min, 4 × 1.5 min, 2 × 5 min, 7–10 × 10 min. The studies were performed at baseline and after pretreatment (blocking studies) with the 5-HT_{2A} antagonists ketanserin (Leysen et al., 1982; Leysen, 1989) or SR 46349B (Rinaldi-Carmona et al., 1992). The studies corresponded to: [^{18}F]altanserin at baseline ($n = 7$) and after either 3–5 mg/kg of ketanserin ($n = 3$) or 1 mg/kg of SR 46349B ($n = 2$); [^{18}F]ALT-ol at baseline ($n = 3$) and after 1 mg/kg of SR46349B ($n = 1$); and [^{18}F]4-FBP at baseline ($n = 3$) and after 1 mg/kg of SR46349B ($n = 1$). No baboon was studied twice with the same radiotracer.

Plasma analyses

Radiolabeled metabolites

An isocratic HPLC method was used to analyze plasma after the injection of either [^{18}F]altanserin, [^{18}F]ALT-ol, or [^{18}F]4-FBP. For the [^{18}F]altanserin and [^{18}F]ALT-ol plasma analyses, a Waters C_{18} Symmetry column was eluted with a mixture of 23% acetonitrile and 77% aqueous buffer (0.29 M acetic acid/0.03 M ammonium acetate, pH 5.2), while an eluent of 15% acetonitrile and 85% aqueous buffer was used for [^{18}F]4-FBP as a result of its relatively shorter retention time. Plasma metabolites were determined from heparinized arterial whole blood (2 ml) centrifuged for 2 min at 13,000*g*. The resulting plasma supernatant (0.5 mL) was added to a solution (10 mL) of 50 mM acetic acid and 5.6 μg carrier (nonradioactive) altanserin and eluted through a Waters C_{18} Sep-Pak Light cartridge. Radioactivity was quantitatively retained on the cartridge (>90%) and the cartridge was sequentially eluted with aqueous 0.1% triethylamine (5 mL), water (5 ml), and methanol (1.5 ml). Methanol removed more than 98% of the radioactivity from the cartridge, while the aqueous triethylamine and water washes removed less than 2% of the radioactivity. The methanol eluent was passed through a Millipore HV syringe filter and injected onto a Waters analytical μBondapak C_{18} HPLC column. HPLC eluent fractions (2 ml) were collected and counted in a gamma counter (Packard™ 5010).

Input function determination

Two types of plasma input functions were determined and corresponded to the concentrations of: 1) unmetabolized parent radiotracer (C_p: either [^{18}F]altanserin, [^{18}F]ALT-ol, or [^{18}F]4-FBP injectate); and 2) all radiolabeled metabolites ($C_{p\text{-}MET}$) in plasma. Input functions were comprised of approximately 20 arterial blood samples (0.5 ml) over the initial 2 min after radiotracer injection followed by an additional 15–20 samples for the remainder of the study. After centrifugation of the samples, 200 μl of plasma were removed and the plasma radioactivity concentrations were determined using a COBRA™ Auto-Gamma® model 5003 gamma counter (Packard Instruments, Meriden, CT). The radioactivity in each sample was corrected for radioactive decay and converted to units of μCi/ml using the well counter sensitivity and sample size values.

Additional arterial blood samples were obtained at five or six time points during the study (2, 10, 30, 60, 90, and 120 min) for the determination of radiolabeled metabolites in plasma using reverse-phase HPLC (see above). These data yielded values of the unchanged fraction of parent radiotracer (relative to the total plasma radioactivity) throughout the time frame of the study. A multiexponential equation was used to describe this curve and to estimate the parent fraction at each measured plasma curve time point (metabolite correction factors). The metabolite-corrected input function was calculated by multiplication of the total plasma radioactivity concentration by the metabolite correction factors. The metabolite input function used in the present work ($C_{p\text{-}MET}$) corresponded to the total concentration of radiometabolites in plasma and was determined as the difference between the total ($C_{p\text{-}TOT}$) and parent (C_p) plasma radioactivity concentrations.

Data analyses

Region-of-interest definition

Circular (1 cm diameter) regions-of-interest (ROIs) were drawn on summed PET images (0–15 min postin-

*TABLE I. Compartmental modeling: nonspecific component**

Single Input	1. Parent Radiotracer only (C_p)	
2C	1 Tissue compartment:	K_1, k_2, and V_V term
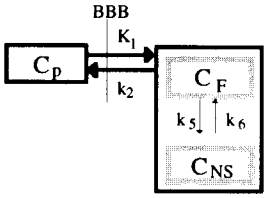	2C DV = K_1/k_2	
3C$_{NS}$	2 Tissue compartments:	K_1, k_2, k_5, k_6, and V_V term
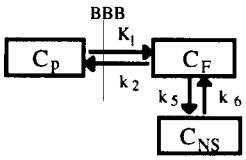	3C$_{NS}$ DV = $K_1/k_2(1+ k_5/k_6)$	
	DV$_{NS}$ = $K_1/k_2(k_5/k_6)$ for negligible specific binding	
Dual Input	1. Parent Radiotracer (C_p) and 2. Radiolabeled Metabolites ($C_{p\text{-}MET}$)	
2C+2C$_{MET}$	2 Tissue compartments:	K_1, k_2, $K_{1\text{-}MET}$, $k_{2\text{-}MET}$, and V_V
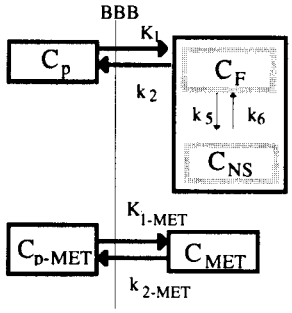	Constraint:	$K_{1\text{-}MET} = K_1$
	2C DV = K_1/k_2	
	DV$_{MET}$ = $K_{1\text{-}MET}/k_{2\text{-}MET}$	

*See Methods, Data analyses sections.

jection) and applied to the dynamic PET images to generate time–activity curves for the frontal (FRT) and temporal (TEM) cortices, striatum (STR), and cerebellum (CER). The ROIs were created using Imagetool™ software (CTI PET Systems). The regional PET time–activity data were generated using an internally developed Interactive Data Language (Research Systems, Boulder, CO) routine that utilized a phantom-based calibration factor to convert that PET data units into units of μCi/ml (see Drevets et al., 1999).

Compartmental analyses

The data were analyzed using single (conventional) and dual (conventional + metabolite) input function models. All model configurations are described in Table I. The analyses focused on the kinetics of the concentrations of free and nonspecific radioactivity in brain. Therefore, the models described below do not include a specific binding compartment.

The PET measurement was described in terms of the tissue concentrations of parent radiotracer (C_F, C_{NS}) and radiolabeled metabolites (C_{MET}). The terms C_F and C_{NS} refer to the concentrations of free and nonspecifically-bound parent radiotracer in brain, respectively (see Koeppe et al., 1994), while C_{MET} denotes the radioactivity concentration of radiolabeled metabolites in brain. The input functions to the compartmental model(s) corresponded to the concentrations of parent radiotracer (C_p) and radiolabeled metabolites ($C_{p\text{-}MET}$).

In the model equations shown below, bidirectional BBB transport was represented by K_1 (ml/min/ml) and k_2 (min^{-1}) and association and dissociation rates of nonspecific binding by k_5 (min^{-1}) and k_6 (min^{-1}). The parameters $K_{1\text{-}MET}$ (ml/min/ml) and $k_{2\text{-}MET}$ (min^{-1})

represented the bidirectional transport of radiometabolites from plasma into brain (C_{MET}). The model equations were:

$$\frac{dC_F(t)}{dt} = K_1C_p(t) - (k_2 + k_5)C_F(t) + k_6C_{NS}(t) \quad (1)$$

$$\frac{dC_{NS}(t)}{dt} = k_5C_F(t) - k_6C_{NS}(t) \quad (2)$$

$$\frac{dC_{MET}(t)}{dt} = K_{1\text{-}MET}C_{p\text{-}MET}(t) - k_{2\text{-}MET}C_{MET}(t) \quad (3)$$

and the total model solution (C_{MOD}) was:

$$C_{MOD} = C_F + C_{NS} + C_{MET} + V_V(C_{p\text{-}TOT}) \quad (4)$$

The total solution included a vascular volume (V_V) term to account for the contribution of vascular radioactivity to the PET signal; V_V was determined as a fractional amount of the total plasma radioactivity concentration ($C_{p\text{-}TOT}$).

When only the parent radiotracer was considered in brain (single input, Eq. 4, $C_{MET}(t) = 0$), the configurations corresponded to either 2- or 3-compartment models (2C or 3C). The 2C and 3C models consisted of one vascular compartment (C_p) and one ($C_F + C_{NS}$) or two (C_F, C_{NS}) tissue compartments, respectively. In this work, the 3C model was denoted as $3C_{NS}$ because it was applied to examine the kinetics of the nonspecific (NS) radioactivity.

When the contribution of radiometabolites was also considered in brain (dual input, Eq. 4, $C_{MET}(t) \neq 0$), the model configuration included a parallel component that allowed for BBB transport of radiolabeled metabolites. The parallel component consisted of one vascular compartment ($C_{p\text{-}MET}$) and one tissue compartment (C_{MET}). Thus, the dual-input configuration was a combination of the single-input 2C model and a 2C metabolite model ($2C + 2C_{MET}$), as has been similarly described and implemented for other PET studies (Huang et al., 1991; Votaw et al., 1993; Price et al., 1996, 1998; Burger and Buck, 1996).

In this study of baboons, the MET term denoted the use of all measured plasma metabolites (in contrast to the use of only BBB-permeable metabolites: MET′, see Part II companion article: Price et al., 2001). No analysis accounted for the metabolism of radiotracer in brain (Gunn et al., 2000) because previous animal studies in our laboratory did not indicate that this would be a significant issue (Smith et al., 1998; unpublished data).

Curve fitting

The kinetic parameters were estimated using an iterative least-squares curve fitting technique (Bevington, 1969; Press et al., 1986) and the minimization method of Marquardt (1963). The parameter standard errors were determined using the diagonal components of the covariance matrix (Bevington, 1969). Comparisons were made between the compartmental models using the Akaike information criteria (AIC) for which the lowest value indicated the model that provided the best fit to the data (Akaike, 1974).

The kinetic parameters were used to calculate radiotracer distribution volume (DV) measures (Table I). The DV is a measure of tissue radioactivity localization (see Koeppe et al., 1994). The single-input $3C_{NS}$ model was applied to the PET data to assess the DV of the nonspecific component, $DV_{NS} = K_1/k_2(k_5/k_6)$. In addition, the dual-input model provided an estimate of the DV of radiolabeled metabolites, $DV_{MET} = K_{1\text{-}MET}/k_{2\text{-}MET}$. All kinetic parameters were allowed to vary freely during the single-input 2C and $3C_{NS}$ model fits. For the dual-input model, curve fits were performed with all parameters freely varying or with $K_{1\text{-}MET}$ fixed to K_1 (Mintun et al., 1996).

RESULTS

[^{18}F]Altanserin, [^{18}F]ALT-ol, and [^{18}F]4-FBP Imaging

Figure 1 shows PET images acquired in the same baboon following injection of [^{18}F]altanserin, [^{18}F]ALT-ol, or [^{18}F]4-FBP (across four brain slices). The brain uptake after injection of [^{18}F]altanserin was greater than that after [^{18}F]ALT-ol or [^{18}F]4-FBP with percent injected dose/ml measures in the frontal cortex of 0.014%, 0.004%, and 0.010%, respectively, at 25 min. The early [^{18}F]altanserin and [^{18}F]4-FBP images (0–8 min) show radiotracer uptake that is more consistent with the distribution of blood flow than with 5-HT$_{2A}$ receptor binding, while the early [^{18}F]ALT-ol images reflect low overall radiotracer uptake in brain that is difficult to visualize as a result of greater levels of radioactivity outside of the brain. In contrast, the later [^{18}F]altanserin images (35–90 min postinjection) displayed radioactivity concentrations that followed a rank order that was consistent with regional 5-HT$_{2A}$ receptor binding: frontal and temporal cortices > thalamus > basal ganglia > cerebellum. Regionally specific 5-HT$_{2A}$ receptor binding was not evident in the later [^{18}F]ALT-ol or [^{18}F]4-FBP image data (see below, Tissue ratios). These data were consistent with BBB passage and nonspecific localization of [^{18}F]ALT-ol, [^{18}F]4-FBP, and/or their secondary radiolabeled metabolites.

Plasma analyses

Following the bolus injection of [^{18}F]altanserin in baboons, the isocratic HPLC method resulted in the separation of unchanged [^{18}F]altanserin and two other major radiolabeled components (Price et al., 1998). This method yielded 88 ± 5% and 23 ± 8% of the total plasma radioactivity as [^{18}F]altanserin at 2 and 90 min, respectively. Of the two major radiolabeled com-

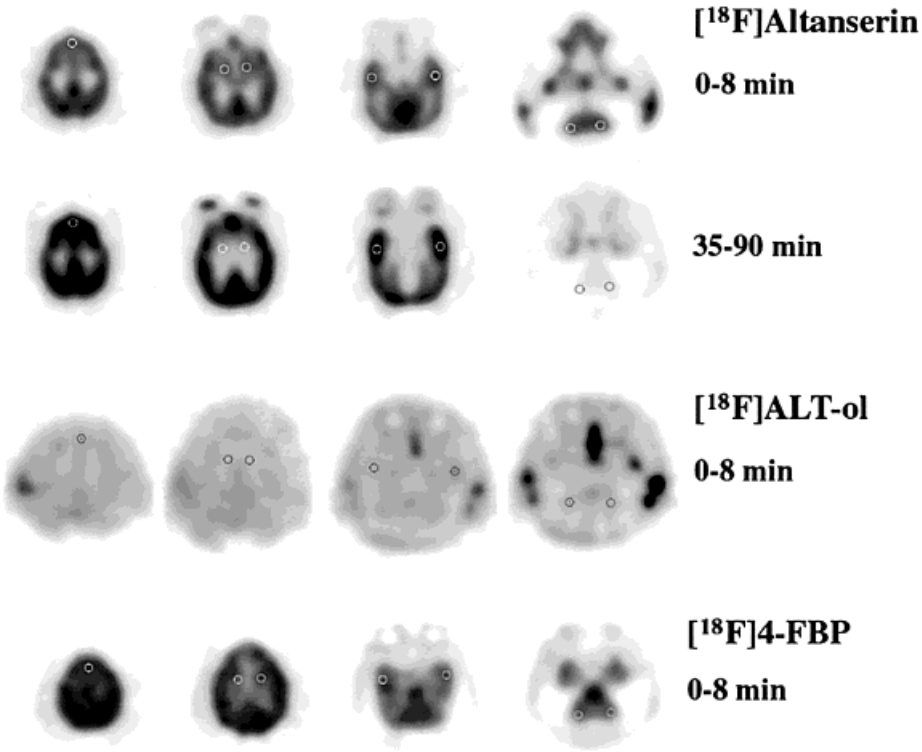

Fig. 1. Summed PET images of [^{18}F]altanserin, [^{18}F]ALT-ol, and [^{18}F]4-FBP. These images represent the summed radioactivity distribution of [^{18}F]altanserin (first and second rows), [^{18}F]ALT-ol (third row), and [^{18}F]4-FBP (fourth row) in the same baboon. Each radiotracer image set was scaled to its own maximum (darkest) value. The images depict four brain levels and ROIs (FRT, STR, TEM, CER, see Methods for definitions). The [^{18}F]altanserin images (35–90 min postinjection) displayed radioactivity concentrations that were consistent with 5-HT$_{2A}$ receptor binding: frontal and temporal cortices > thalamus > basal ganglia > cerebellum. Specific 5-HT$_{2A}$ receptor binding was not evident for any region or at any time after [^{18}F]ALT-ol or [^{18}F]4-FBP injection.

ponents, one was longer-retained, more lipophilic (contained [^{18}F]ALT-ol), and accounted for approximately 2% and 12% of the total plasma radioactivity at 2 and 90 min, respectively. The shorter-retained component was more polar (contained [^{18}F]4-FBP and its primary metabolite, [^{18}F]4-FBPmet) and accounted for about 10% and 50% at 2 and 90 min, respectively.

Figure 2 (left graphs) displays the plasma input functions that correspond to 1) unmetabolized parent radiotracer, and 2) all radiolabeled metabolites that were measured after the bolus injection of [^{18}F]altanserin, [^{18}F]ALT-ol, or [^{18}F]4-FBP. At early times after [^{18}F]altanserin injection, the proportion of the injected parent radioactivity in plasma was greater than that observed after [^{18}F]ALT-ol or [^{18}F]4-FBP injection with the highest levels of radiolabeled metabolites measured after [^{18}F]4-FBP injection (Fig. 2, left graphs).

Tissue ratios

Tissue ratios were computed for the frontal cortex (FRT) and cerebellar (CER) PET data relative to the concentrations of unmetabolized parent (C_p) in plasma. In addition, the FRT data were expressed relative to the CER data. Figure 2 (right graphs) displays average tissue ratios that were determined across baboons after the injection of either [^{18}F]altanserin, [^{18}F]ALT-ol, or [^{18}F]4-FBP. After [^{18}F]altanserin injection, the CER/C_p ratios plateaued at a value of approximately 3 after 20 min. The [^{18}F]altanserin FRT/C_p ratios exhibited a transient plateau near 9 (60–80 min). However, the FRT/CER ratios were 3-fold lower than the FRT/C_p values and yielded a more distinct plateau near a value of 3 after 70 min. The [^{18}F]altanserin tissue ratio results were consistent with high levels of nonspecific binding in brain and/or BBB passage of radiometabolites of [^{18}F]altanserin.

In contrast to [^{18}F]altanserin, the bolus injection of [^{18}F]ALT-ol or [^{18}F]4-FBP yielded regional tissue-to-plasma ratios that were fairly uniform across regions and, thus, not consistent with the rank order of 5-HT$_{2A}$ receptor binding. For example, after the injection of either [^{18}F]ALT-ol or [^{18}F]4-FBP, the FRT/CER values were nearly 1 by 10–20 min. Of note were the large tissue-to-plasma ratios observed after [^{18}F]4-FBP injection. The substantial metabolic activity in plasma and the large tissue ratios observed after [^{18}F]4-FBP injection were consistent with the BBB passage of [^{18}F]4-FBP and/or radiolabeled metabolites of [^{18}F]4-FBP ([^{18}F]4-FBPmet).

After pharmacologic receptor blockade, the FRT/CER tissue ratios were consistent with nonspecific localization of radiotracer (lack of 5-HT$_{2A}$ receptor rank order). For example, the FRT/CER value after SR46349B pretreatment was about 1.3, 0.4, or 1.0 after the injection of [^{18}F]altanserin, [^{18}F]ALT-ol, or [^{18}F]4-FBP injection, respectively. The [^{18}F]ALT-ol and [^{18}F]4-FBP FRT/CER values were less than or close to 1 at baseline and after receptor blockade.

Compartmental analyses

The compartmental analyses were focused on [^{18}F]altanserin cerebellar and blocking data and baseline

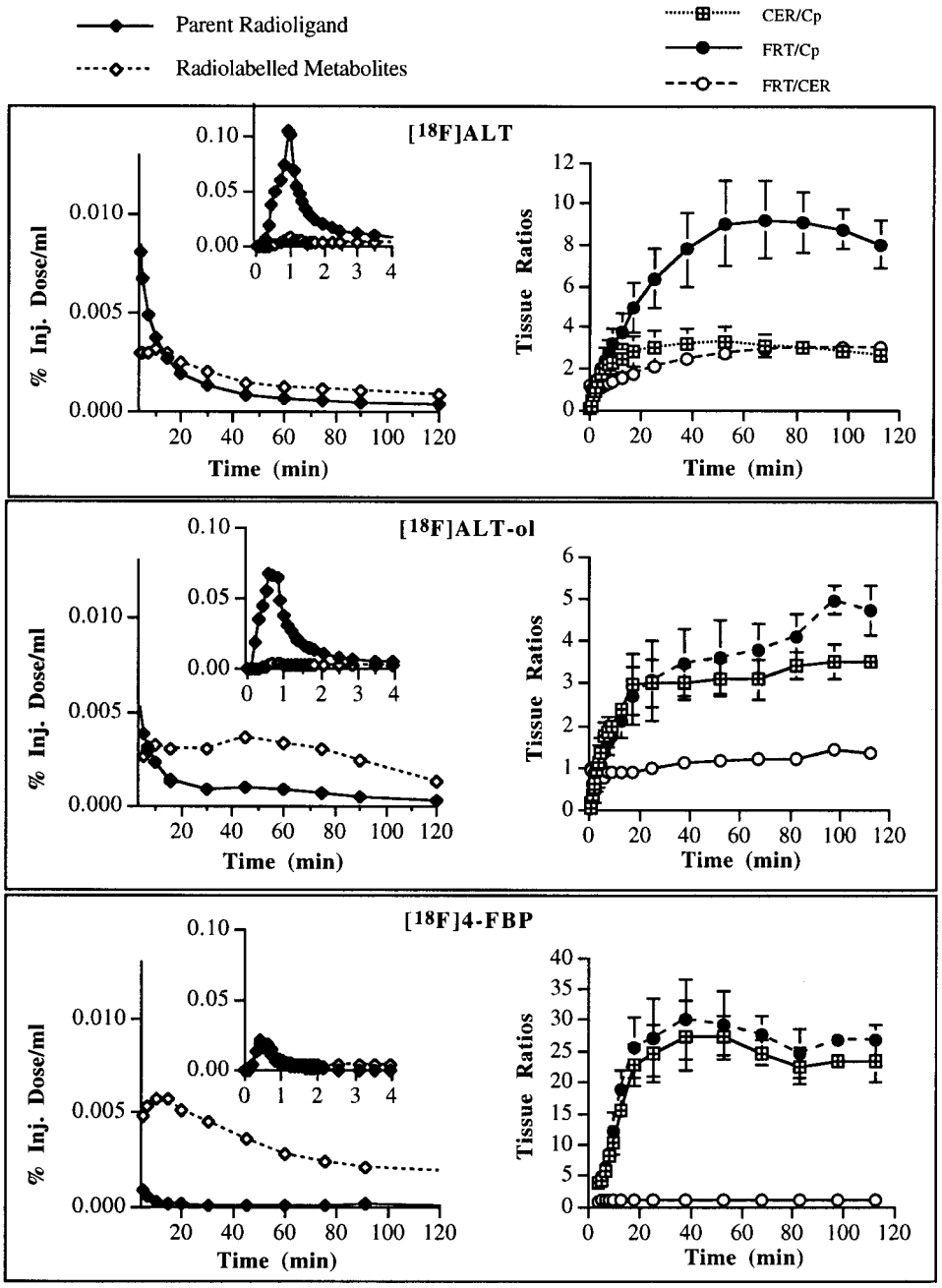

Fig. 2. Plasma radioactivity concentrations (left graphs) measured in baboon after i.v. injection of either: [18F]altanserin ([18F]ALT, top), [18F]ALT-ol (middle), or [18F]4-FBP (bottom). The graphs show the percentage of the injected dose per ml of plasma (%Inj. Dose/ml) for the parent radiotracer (solid diamonds) and total radiolabeled metabolites (open diamonds) at early (inset graph) and late postinjection times after injection. The lowest %Inj. Dose/ml values were found for [18F]4-FBP and substantial metabolic activity was observed following [18F]4-FBP injection. The right column of graphs shows tissue ratios (mean ± SD) for [18F]ALT (top), [18F]ALT-ol (middle), and [18F]4-FBP (bottom) in baboons. Ratios were determined for the cerebellar data relative to plasma (CER/C_p, crossed squares) and for the frontal data relative to plasma (FRT/C_p, solid circles) and cerebellar data (FRT/CER, open circles). After [18F]ALT injection, CER/C_p began to plateau early at a value of 3, while the FRT/C_p plateau was later and more variable at a value of about 9. The [18F]ALT FRT/CER values yielded a more distinct plateau near 3. In contrast, the injection of [18F]ALT-ol or [18F]4-FBP yielded CER/C_p and FRT/C_p values that were similar and not consistent with the regional rank order of 5-HT_{2A} receptor binding. The injection of either [18F]ALT-ol or [18F]4-FBP led to FRT/CER values of nearly 1; the largest tissue-to-plasma ratios were observed after [18F]4-FBP injection.

[18F]ALT-ol and [18F]4-FBP data. This focus was primarily the result of our interest in the [18F]altanserin nonspecific component and because we previously examined regional baseline [18F]altanserin data in baboons (Price et al., 1998). The compartmental analyses of the [18F]ALT-ol and [18F]4-FBP data were limited to a subset of studies as a result of complexities that arose in data preparation (see below).

The application of the dual-input (conventional + metabolite) compartmental model to the baboon studies utilized a metabolite input function that was comprised of all radiolabeled metabolites (MET). For [18F]altanserin, this was not precise because not all of its radiolabeled metabolites were found to cross the BBB (Smith et al., 1998; Part II companion article: Price et al., 2001). For the dual-input analyses of [18F]ALT-ol and [18F]4-FBP, the metabolite input function also consisted of all radiometabolites in plasma because an extensive in vivo characterization of the radiometabolites that arise after the bolus injection of [18F]ALT-ol or [18F]4-FBP has not been performed.

For [18F]ALT-ol, compartmental modeling was troublesome at baseline and particularly after pharmacologic blockade, primarily because its low brain uptake made ROI definition difficult. In addition, it was possible that some of the [18F]ALT-ol would be converted

*TABLE II. Evaluation of nonspecific binding in baboons**

	CER ALT (n = 7)	CER KETAN + ALT (n = 3)	FRT KETAN + ALT (n = 3)	CER ALT-ol (n = 3)	FRT ALT-ol (n = 3)	CER 4-FBP (n = 1)	FRT 4-FBP (n = 1)
Single Input							
$2C$ DV	1.64 ± 0.42	1.80 ± 0.31	1.64 ± 0.42	1.92 ± 0.16	2.36 ± 0.43	20.59	21.88
AIC	9 ± 24	2 ± 9	7 ± 3				
$3C_{NS}$ DV	1.85 ± 0.52	1.93 ± 0.34	1.59 ± 0.57				
K_1/k_2	1.12 ± 0.26	1.29 ± 0.32	1.48 ± 0.29				
DV_{NS}	0.73 ± 0.30	0.69 ± 0.22	0.66 ± 0.19				
AIC	−48 ± 22	−48 ± 10	−38 ± 11				
Dual Input							
$2C$ + $2C_{MET}$ No constraints							
K_1/k_2	1.15 ± 0.27	1.40 ± 0.37	1.55 ± 0.41				
DV_{MET}	0.67 ± 0.58	0.51 ± 0.18	0.49 ± 0.15				
AIC	−20 ± 21	−11 ± 16	−6 ± 21				
$2C$ + $2C_{MET}$ Constraint: $K_{1\text{-}MET} = K_1$							
K_1/k_2	0.92 ± 0.29	1.23 ± 0.35	1.32 ± 0.45				
DV_{MET}	0.90 ± 0.62	0.69 ± 0.17	0.65 ± 0.17				
AIC	−31 ± 22	−25 ± 3	−22 ± 10				

*ALT: [^{18}F]altanserin; KETAN: ketanserin; ALT-ol: [^{18}F]ALT-ol; 4-FBP: [^{18}F]4-FBP.
Modeling was performed for one baseline [^{18}F]4-FBP study (see Results, Compartmental modeling sections).

into [^{18}F]altanserin, analogous to the slow conversion of ketanserin-ol to ketanserin reported in rats and humans (Van Peer et al., 1986; Heykants et al., 1986), but the extent of this conversion in baboons did not appear to greatly complicate the compartmental results over the time frame of the study. Lastly, after bolus injection, [^{18}F]4-FBP was rapidly metabolized in vivo with evidence of rapid BBB passage of [^{18}F]4-FBP and/or its radiolabeled metabolites (unpublished data). This rapid metabolism in plasma complicated the accurate determination of the [^{18}F]4-FBP input function and limited our compartmental analysis to one baseline [^{18}F]4-FBP baboon study, although more studies were performed and presented in the Tissue ratio section (above).

Nonspecific binding

The [^{18}F]altanserin cerebellar data were not well described by the $2C$ model (underestimation at early times) and were best described by the $3C_{NS}$ model (lowest AIC values), whether at baseline or after ketanserin pretreatment (Table II). The $3C_{NS}$ model also performed better than the $2C$ model for data from receptor-rich regions after ketanserin pretreatment (Table II, FRT results). Low AIC values (relative to the $2C$ model) also were found for the $2C$ + $2C_{MET}$ model fits. The $3C_{NS}$ and $2C$ + $2C_{MET}$ analyses were sometimes hindered by large parameter errors (>50%) that were observed for the $3C_{NS}$ k_6 parameter and the $2C$ + $2C_{MET}$ DV_{MET} parameter, although the $2C$ + $2C_{MET}$ model performed better when constrained (relative to unconstrained). The failure of the $2C$ model and the better performance of the $3C_{NS}$ model indicated the existence of more than one tissue component in the [^{18}F]altanserin baseline cerebellar and ketanserin-blocked PET data.

The average [^{18}F]altanserin cerebellar $3C_{NS}$ nonspecific component ($DV_{NS} = K_1/k_2 * k_5/k_6$) was similar to the DV_{MET} value of the dual-input model, at baseline or after ketanserin pretreatment (Table II). This similarity was also observed in the receptor-rich frontal region after ketanserin pretreatment (Table II, FRT results) and further suggested the presence of a nonspecific radioactivity "background" to which radiolabeled metabolites of [^{18}F]altanserin contributed.

The results of the [^{18}F]ALT-ol studies yielded $2C$ DV values for the CER and FRT regions that were not greatly different than the [^{18}F]altanserin DV value obtained by the $3C_{NS}$ model (Table II). However, the average [^{18}F]ALT-ol FRT DV was greater than the average CER DV by about 20%. The latter observation was consistent with reports of a slow oxidative conversion of [^{18}F]ALT-ol to [^{18}F]altanserin in vivo during the time frame of the study, both in rats (Lopresti et al., 1998) and baboons (unpublished data). If slow oxidative conversion occurred, low levels of [^{18}F]altanserin specific binding might have existed in the [^{18}F]ALT-ol FRT data. Overall, the [^{18}F]ALT-ol data were best described by the single-input $2C$ model (lowest AIC value), as large standard errors arose (>50%) in the $3C_{NS}$ model parameters and in the $2C$ + $2C_{MET}$ DV_{MET} parameters (data not shown).

The results of the compartmental analyses of the [^{18}F]4-FBP data were consistent with the tissue ratio data and with significant nonspecific binding that was likely the result of BBB passage of radiometabolites after [^{18}F]4-FBP injection (Fig. 2). Similar to [^{18}F]ALT-ol, the [^{18}F]4-FBP data were well described by the

single-input 2*C* model with poor performance by the $3C_{NS}$ or $2C + 2C_{MET}$ model (inadequate description of the data and large parameter errors). For one [18F]4-FBP baboon, the 2*C DV* value was similar for the CER and FRT regions (Table II) and about 10 times larger than the average [18F]ALT-ol 2*C DV* value.

DISCUSSION

The primary goal of this work was to further characterize the in vivo metabolism and kinetics of [18F]altanserin and its radiometabolites in baboons. First, the results demonstrated BBB passage and nonspecific localization of tissue radioactivity after the bolus injection of each of two identified metabolites of [18F]altanserin. Second, the conventional measure of the slow [18F]altanserin nonspecific component was similar to the metabolite component that was measured by the dual-input method in receptor-rich and receptor-poor regions.

Localization of BBB metabolites

Radioactivity in brain after [18F]ALT-ol and [18F]4-FBP injection in baboon was nonspecifically distributed. The baseline [18F]altanserin tissue ratios were consistent with 5-HT_{2A} receptor binding (FRT > CER, Price et al., 1998), while no regional order was observed after ketanserin or SR46349B pretreatment. Evidence of nonspecific localization was found in the FRT/CER tissue ratios for [18F]ALT-ol and [18F]4-FBP that did not exhibit 5-HT_{2A} receptor rank order, whether at baseline or after SR46349B pretreatment. Evidence of nonspecific localization of brain radioactivity after [18F]4-FBP injection was particularly important because of its rapid metabolism in plasma and because the brain radioactivity was substantial. Further, the compartmental results supported the tissue ratio findings. The better performance of the $3C_{NS}$ and dual-input models (relative to the 2*C* model) for the [18F]altanserin data indicated a nonspecific tissue component to the cerebellar and ketanserin-blocked regional PET data that could partly result from BBB passage of radiolabeled metabolites.

Nonspecific binding component

The [18F]altanserin nonspecific component (DV_{NS}) that was measured by the $3C_{NS}$ analysis did not appear to be different from the metabolite component (DV_{MET}) that was measured by the dual-input function analysis (Table II). In addition, the blocking data showed that the value did not appear to be different for the receptor-rich frontal cortex and the receptor-poor cerebellum. These observations suggest that the nonspecific localization of [18F]ALT-ol and [18F]4-FBP (and/or their BBB-permeable metabolites) at later times is fairly uniform across regions. Regionally constant nonspecific localization of [18F]altanserin radiometabolites would be consistent with a recent human equilibrium PET study for which a cerebellar subtraction method was applied to the regional data to correct for radiolabeled metabolites (van Dyck et al., 2000).

Study limitations

Human autoradiographic studies have shown that low levels of 5-HT_{2A} receptors exist in the cerebellum (Pazos et al., 1987). Therefore, it is important to acknowledge that low levels of cerebellar 5-HT_{2A} receptor binding may contribute bias to the [18F]altanserin results. However, we do not expect that the [18F]altanserin results were significantly impacted by 5-HT_{2A} receptor binding in the cerebellum given the fairly comparable *DV* measures that were obtained for the cerebellum at baseline and after pharmacologic receptor blockade. In addition, large errors were sometimes associated with the [18F]altanserin DV_{MET} parameter in this study. The large errors could have reflected that a more specific characterization of the radiolabeled metabolites was needed since all radiolabeled metabolites of [18F]altanserin do not cross the BBB in rats (Smith et al., 1998). Therefore, our evaluation of [18F]altanserin bolus injection data in humans will build on the results of the baseline and blocking studies in baboons and utilize a more specific characterization of the radiolabeled metabolites of [18F]altanserin in plasma (Smith et al., 1998; Tan et al., 1999; Part II companion article: Price et al., 2001).

CONCLUSIONS

The results of this study indicated nonspecific tissue localization of radiolabeled metabolites of [18F]altanserin. The tissue contribution of the radiolabeled metabolites could result in an overestimation of the [18F]altanserin nonspecific component by conventional (single-input function) methods. We found that the nonspecific component was comparable in receptor-poor and receptor-rich regions and this result strengthened the validity of previous analyses of bolus injection [18F]altanserin PET data by conventional methods. The results of the present baboon studies are essential for the evaluation and interpretation of human bolus injection [18F]altanserin PET data, for which pharmacologic receptor blockade is not practical.

ACKNOWLEDGMENTS

The authors thank the University of Pittsburgh PET facility staff in conducting the experiments: Marsha Martinelli, C.N.M.T.; James Ruszkiewicz, C.N.M.T.; Donna Milko, C.N.M.T.; Denise Ratica, C.N.M.T.; Jennifer Perevuznik, B.S.; David Manthei, B.S.; Louise Smith, R.N.; Doug Parkinson, R.N.; Phil Greer, B.A.; and Robert Sembrat, B.S.

REFERENCES

Akaike H. 1974. A new look at the statistical model identification. IEEE Trans Automat Control 19:716–723.

Bevington PR. 1969. Data reduction and error analysis for the physical sciences. New York: McGraw-Hill. p 204–246.

Biver F, Goldman S, Luxen A, Monclus M, Forestini M, Mendlewicz J, Lotstra F. 1994. Multicompartmental study of fluorine-18 altanserin binding to brain $5HT_2$ receptors in humans using positron emission tomography. Eur J Nucl Med 21:937–946.

Burger C, Buck A. 1996. Tracer kinetic modelling of receptor data with mathematical metabolite correction. Eur J Nucl Med 23:539–545.

Drevets WC, Price JC, Kupfer DJ, Kinahan PE, Lopresti B, Mathis C. 1999. PET measures of amphetamine-induced dopamine release in ventral versus dorsal striatum. Neuropsychopharmacology 21:694–709.

Gunn RN, Yap JT, Wells P, Osman S, Price P, Jones T, Cunningham VJ. 2000. A general method to correct PET data for tissue metabolites using a dual scan approach. J Nucl Med 41:706–711.

Heykants J, Van Peer A, Woestenborghs R, Gould S, Mills J. 1986. Pharmacokinetics of ketanserin and its metabolite ketanserin-ol in man after intravenous, intramuscular and oral administration. Eur J Clin Pharmacol 31:343–350.

Heykants J, Michiels M, Woestenborghs R, Awouters F, Leysen JE, Schuurkes J. 1988. Pharmacokinetic evaluation of the in vitro and in vivo pharmacological profile of the major metabolites of ketanserin in the rat. Arzneim-Forsch/Drug Res 38(I).

Huang S-C, Yu D-C, Barrio JR, Grafton S, Melega WP, Hoffman JM, Satyamurthy N, Mazziotta JC, Phelps ME. 1991. Kinetics and modeling of L-6-[^{18}F]fluoro-DOPA in human positron emission tomographic studies. J Cereb Blood Flow Metab 11:898–913.

Koeppe RA, Frey KA, Mulholland GK, Kilbourn MR, Buck A, Lee KS, Kuhl DE. 1994. Tropanyl benzilate-binding to muscarinic cholinergic receptors: methodology and kinetic modeling alternatives. J Cereb Blood Flow Metab 14:85–89.

Lemaire C, Cantineau R, Guillaume M, Plenevaux A, Christiaens L. 1991. Fluorine-18-altanserin: a radioligand for the study of serotonin receptors with PET: radiolabeling and in vivo biologic behavior in rats. J Nucl Med 32:2266–2272.

Leysen JE. 1989. Use of $5\text{-}HT_2$ receptor agonists and antagonists for the characterization of their respective receptor sites. In: Boulton A, Baker C, Juorio A, editors. Drugs as tools in neurotransmitter research. Totowa, NJ: Humana Press. p 299–350.

Leysen JE, Niemegeers CJE, Van Nueten JM, Laduron PM. 1982. ^{3}H-ketanserin (R 41 468), a selective ligand for serotonin$_2$ receptor binding sites. Binding properties, brain distribution and functional role. Mol Pharmacol 21:301–304.

Lopresti B, Holt D, Mason N, Huang Y, Ruszkiewicz J, Perevuznik J, Price J, Smith G, Mathis C. 1998. Characterization of the radiolabeled metabolites of [F-18]altanserin: implications for kinetic modeling. In: Carson R, Daube-Witherspoon M, Herscovitch P, editors. Quantitative functional brain imaging with PET. San Diego: Academic Press. p 293–298.

Marquardt DW. 1963. An algorithm for least squares estimation of nonlinear parameters. J Soc Ind Appl Math 2:431–441.

Mason NS, Huang Y, Holt D, Perevuznik J, Lopresti B, Mathis C. 1997. Synthesis of two radiolabeled metabolites of [F-18]altanserin. J Label Comp Radiopharm 40:161–162.

Mintun MA, Price JC, Smith GS, Lopresti B, Hartman L, Simpson N, Mathis CA. 1996. Quantitative $5\text{-}HT_{2A}$ receptor imaging in man using F-18 altanserin: a new model accounting for labeled metabolites. J Nucl Med 37(5):P109.

Pazos A, Probst A, Palacios JM. 1987. Serotonin receptors in the human brain. IV. Autoradiographic mapping of serotonin-2 receptors. Neuroscience 21:123–139.

Press WH, Flannery BP, Teukolsky SA, Vetterling WT. 1986. Numerical recipes: the art of scientific computing. Cambridge, UK: Cambridge University Press.

Price JC, Mathis CA, Simpson NR, Mahmood K, Mintun MA. 1996. Kinetic modeling of serotonin-1A binding in monkeys using ^{11}C WAY 100635 and PET. In: Jones T, et al., editors. Quantification of brain function using PET. San Diego: Academic Press. p 257–261.

Price JC, Lopresti B, Mason S, Huang Y, Holt D, Smith GS, Mathis CA. 1998. [F-18]Altanserin PET studies of serotonin-2A binding: examination of nonspecific component. In: Carson R, Daube-Witherspoon M, Herscovitch P, editors. Quantitative functional brain imaging with PET. San Diego: Academic Press. p 427–434.

Price JC, Lopresti BJ, Meltzer CC, Smith GS, Mason NS, Huang Y, Holt DP, Gunn RN, Mathis CA. 2001. Analyses of [^{18}F]altanserin bolus injection PET data. II. Consideration of radiolabeled metabolites in humans. Synapse.

Rinaldi-Carmona M, Congy C, Santucci V, Simiand J, Gautret B, Neliat G, Labeeuw B, Le Fur G, Soubrie P, Breliere JC. 1992. Biochemical and pharmacological properties of SR 46349B, a new potent and selective 5-hydroxytryptamine2 receptor antagonist. J Pharmac Exp Ther 262:759–768.

Sadzot B, Lemaire C, Maquet P, Salmon E, Plenevaux A, Degueldre C, Hermanne JP, Guillaume M, Cantineau R, Comar D, Franck G. 1995. Serotonin $5HT_2$ receptor imaging in the human brain using positron emission tomography and a new radioligand, [^{18}F]altanserin: results in young normal controls. J Cereb Blood Flow Metab 15:787–797.

Smith GS, Price JC, Lopresti BJ, Huang Y, Simpson N, Holt DP, Mason NS, Meltzer CC, Sweet RA, Nichols TE, Sashin D, Mathis CA. 1998. Test-retest variability of serotonin $5\text{-}HT_{2A}$ receptor binding measured with positron emission tomography and [F-18]altanserin in the human brain. Synapse 30:380–392.

Tan PZ, Baldwin RM, Van Dyck CH, Al-Tikriti M, Roth B, Khan N, Charney DS, Innis RB. 1999. Characterization of radioactive metabolites of $5\text{-}HT_{2A}$ receptor ligand [^{18}F]altanserin in human and rodent. Nucl Med Biol 26:601–608.

van Dyck CH, Tan P-Z, Baldwin RM, Amici LA, Pradeep KG, Ng CK, Soufer R, Charney DS, Innis RB. 2000. PET quantification of $5\text{-}HT_{2A}$ receptors in the human brain: a constant infusion pradigm with [^{18}F]altanserin. J Nucl Med 41:234–241.

Van Peer A, Woestenborghs R, Embrechts L, Heykants J. 1986. Pharmacokinetic approach to equilibrium between ketanserin and ketanserin-ol. Eur J Clin Pharmacol 31:339–342.

Votaw JR, Kessler RM, de Paulis T. 1993. Failure of the three compartment model to describe the pharmacokinetics in brain of a high affinity substituted benzamide. Synapse 15:177–190.